7
Robust and Non-volatile Bipolar Resistive Switching in Sol-gel Derived $BiFeO_3$ Thin Films

7.1 Introduction

In past few years, the demand for non-volatile memory (NVM) with low power requirement, high speed and density has increased in semiconductor industries. Flash NVMs are used extensively for storage but suffers from high writing speed, low speed, low endurance and scaling limit. There are various memory devices such as MRAM, FRAM, PCRAM and RRAM which can be used as next generation NVMs. Among these, RRAMs have attracted considerable attention from research community due to its fast speed, low cost, high density, low power, simple device structure and scaling capability (Waser et al., 2009). It was first discovered by Hickmott in binary oxides in 1962 however; the potential of RRAMs to be used as NVMs are recognized in late 1900s. Since then, RRAM properties are observed in great variety of materials such as TiO_2(Zou et al., 2014), ZnO(Peng et al., 2012), HfO_2(Traore et al., 2015), $BiFeO_3$ (Shuai et al., 2012), and $SmGdO_3$(Sharma et al., 2014). RRAM has a simple MIM capacitor structure. These devices switch sequentially between a high conducting and low conducting states as a function of applied voltage. The origin of RRAM is explained by various switching mechanism such as filament model, interface model, trap assisted model and Mott transition. The filament model explains the formation of conducting filaments between TE and BE and is the most reported switching mechanisms for RRAMs. Here, the device is switched from a low conducting state (HRS) to high conducting states (LRS) and formation of filament is attributed to either metal ion migration or oxygen vacancy migration between TE and BE.

Recently, ME properties of BFO are observed at room temperature where magnetic properties are affected by applied electric field and vice versa(Sun et al., 2015). BFO is synthesized by various deposition techniques; however, BFO shows large leakage current which limits its ferroelectric properties. This high leakage current is attributed to the presence of intrinsic point defects like oxygen vacancies (Tsurumaki et al., 2012)(Huang et al., 2013). Presence of these oxygen vacancies plays an important role in the realization of BFO based RRAM owing to its contribution in filament formation. However, availability of these vacancies depends on the deposition techniques. RRAM devices reported on BFO have shown both unipolar and bipolar characteristics and the origin of its existence is not clear. These films are synthesized by PLD technique which is a high cost vacuum based system. Hence, a low cost deposition technique for BFO needs to be investigated in different electrode configuration to understand the origin of unipolar or bipolar RRAM behaviour.

Sol-gel spin coating method is a simple deposition technique which offers synthesis over large area, control over precursors and low cost to grow different morphologies of BFO. Precursors and solvent play crucial role in growth mechanism of the film and hence choosing the right type of precursors and solvents are important. Spin coated BFO suffers from secondary phase formation because of bismuth loss at higher temperature during annealing, necessary for crystallization. Hence, to avoid aforementioned difficulties; additional mole % of bismuth is

taken to maintain the stoichiometry of the film. Also low temperature is preferred over high temperature to further avoid the bismuth low as well as maintaining the crystallinity.
Hence, reported unipolar and bipolar RRAM behaviour of BFO along with PLD synthesis technique has intrigued us to investigate the RRAM behaviour in sol-gel derived BFO thin film in Ag/$BiFeO_3$/FTO configuration of RRAM devices. Silver as a TE offers better conductivity and may assist in filament formation. FTO as BT offers small difference in work function with (~0.3 eV), allowing easy migration of electrons at BFO/BT junction after application of small electric filed at the BFO/FTO. This device configuration in sol gel deposited BFO has not been reported which encourage us to investigate the RRAM switching characteristics of BFO. Also, there is no report available on the robustness studies of these devices which motivated us to study the ageing influence of the film on RRAM characteristics.

Here, switching characteristics of Ag/BFO/FTO RRAM device is investigated. The device showed stable bipolar RRAM behaviour with large ON/OFF ratio. The observed power consumption and operating set and reset voltages are low. Switching mechanism is probably attributed to metal ion migration assisted filament formation. Robustness studies indicated that devices are still working after 10 months of first device realization, ensuring no degradation.

7.2 Experimental Details

2-methoxyethanol (10 ml) is used to dissolve 0.3 M iron nitrate nonahydrate ($Fe(NO_3)_3.9H_2O$, 98% Alfa Aser) and bismuth nitrate pentahydrate ($Bi(NO_3)_3.5H_2O$, 98% Alfa Aser) to prepare the gel. Further, to compensate the volatilization of bismuth precursor, 3 mol% of additional bismuth precursor is dissolved in the solution. This solution is magnetically stirred at moderated speed for 2 hours at 80 °C to obtain a dark brown solution. The solution is aged overnight to achieve the desired viscosity at room temperature. FTO substrates are cleaned prior to deposition to remove any surface impurities. FTO is sequentially ultra-sonicated in acetone, IPA and DI for 15 minutes each. Finally, the substrates are dried by using nitrogen jet. Substrates are spin coated for 30 sec at 3000 rpm and preheated in open air for 5 minutes at 350 °C on a hot plate. This deposition process is performed twice to get the required thickness. Finally, the obtained BFO film is heated at 450 °C in open air box furnace to achieve the required phase and crystallinity.

Thickness of this film is estimated by using profilometer and the measured thickness is ~70 nm ± 6 nm. Circular silver top contacts are fabricated using thermal evaporation on BFO films. A brass made shadow mask with dimeter and separation 500 µm each is used for contact deposition and the thickness of deposited contact is ~ 300 nm. The device configuration of the BFO RRAM is presented in figure 7.1 (a). Here, positive bias is applied at the TE and BE is grounded, Fig. 7.1(a).

7. 3 Results and Discussion of the Fresh Device

7.3.1 Structural and Microstructural Analysis

Structural information of as deposited film is investigated by Bruker D8 powder diffractometer XRD measurement in lock couple mode. The source of radiation is Cu *Ka* (λ=1.5406 Å) and the instrument is operated at 40.0 kV and 40.0 mA of voltage and current, respectively. The film is scanned between 20°-70° in 2θ range with 0.02°/sec step size. The observed XRD pattern is shown in Fig 7.1(b) for synthesized BFO thin films. The obtained peaks of the pattern are matched well with ICDD # 72-2035 and indicate rhombohedral phase structure of BFO. The film is polycrystalline in nature and no secondary phase peak is observed

indicting phase pure BFO thin film synthesis. The film shows a relative preferred orientation along (012) plane, Fig.7.1(b).

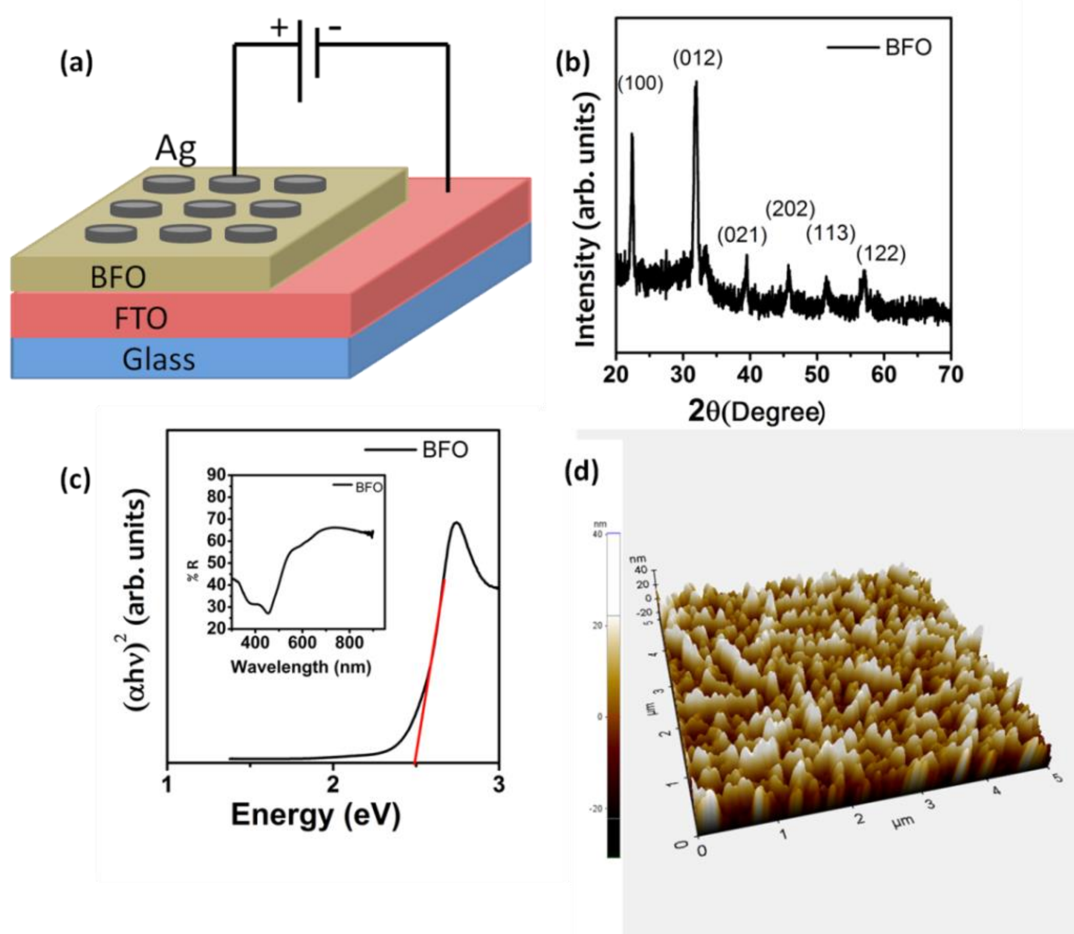

Figure 7.1: (a) Schematic diagram of configuration of Ag/$BiFeO_3$/FTO RRAM device (b) XRD pattern of BFO, (c) Kubelka-Munk plot of BFO and (d) AFM image for BFO thin films

7.3.2 Optical Analysis

The reflectance spectrum is obtained by UV-Vis DRS measurements of the sample and plotted graph is shown in the inset of figure 7.1 (c). It is evident from the graph that film has good reflectance properties. Derived Kubelka-Munk plot is obtained from this data to further calculate the band gap of BFO thin film. A graph between $(\alpha h\nu)^2$ and energy E is shown in figure 7.1 (c). The estimated band gap of BFO thin film is ~ 2.47 eV which is in accordance with reported values. Microstructural information of thin BFO film is analysed using AFM, figure 7.1 (d). AFM results suggest that the films are smooth and estimated roughness (RMS) is 12±0.4 nm. This small roughness may be due to sol-gel synthesis process where crystallization step may produce some surface roughness. However, the film is still relatively smooth and is suitable for device applications.

7.3.3 Electrical Characterization

Keithly 4200-SCS parameter analyser is used to carry out RRAM charactersitics of the synthesized thin BFO film. The configuration of device is presented in Fig. 7.1 (a). Positive bias voltage is applied on TE and negative voltage is applied to BE. I–V results are measured by applying a cyclic voltage in sequence of -2 V→ 0 V→2 V→ 0 V→ -2 V on the Ag/$BiFeO_3$/ FTO device, figure 7.2 (a). Further, 10 mA compliance current is applied on the device in conjunction

with applied voltage in order to prevent the device from external breakdown. The current conduction is taking place from BE to TE in accordance with the applied bias voltage in the BFO thin film based RRAM device. Usually the film is in insulating state at the start hence, a relatively higher bias voltage is applied on the device to achieve a soft breakdown in the device. This process is known as electroforming, and device changes from high resistance to low resistance state due to the filament formation between TE and BE. The electroforming measurement is shown in the inset of figure 7.2 (a). Here, the graph indicates a change in HRS to LRS at forming voltage (V_f) =2.55 V. after electroforming step, relatively low voltage is required to bring the device from HRS to LRS. Further, when a positive voltage sweep is applied from 0-2V, the current starts increasing and resistance starts decreasing, finally sudden increase in current is noted at 1.15 V. This process brings the device from HRS to LRS and turns the device on, bringing the device in set state. The voltage at which set is observed is known as set voltage (V_{set}). The device sustains its LRS in 2-0V sweep range. Further, in negative bias region, compliance free voltage sweeping is applied from 0 to -2 V. Here, the current starts decreasing from higher to lower value at around -1.5 V. This increase in resistance is attributed to the switching of states from LRS to HRS and is refereed as reset process. The device maintains its HRS during voltage sweep from -2 V to 0. The estimated *Ion/Ioff* ratio of these RRAM devices is more than 450. Here the change in states from set to reset depends on the polarity of applied voltage sweep, substantiating the bipolar behaviour of the devices.

The device is tested for its reproducibility and switching is carried out for 100 cycles and the graph is shown in figure 7.2 (b). These results confirm that devices are reproducible and stable throughout the measurements.

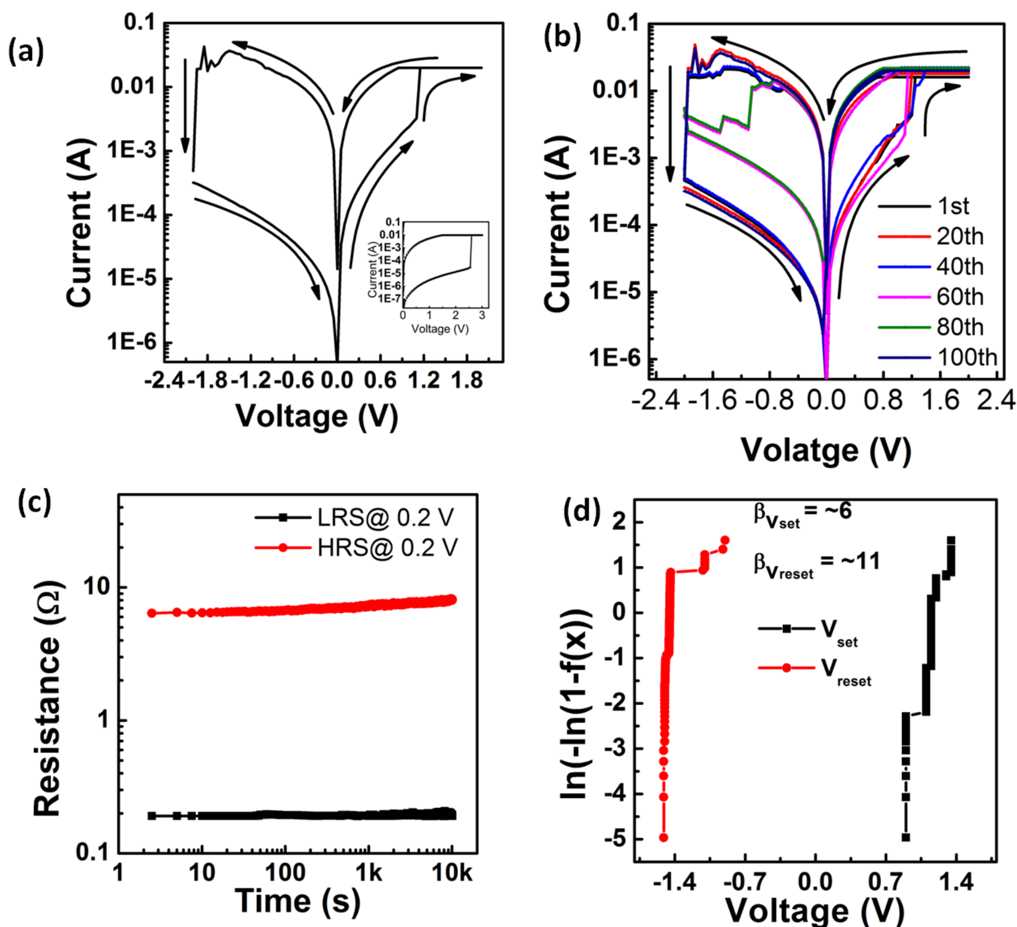

Figure 7.2: (a) First RRAM switching cycle, (b) Switching curve of 100 cycles, (c) Retention curve, and (d) Reliability of set and reset voltage

Retention study of these devices is performed at room temperature for 10^4 seconds in LRS and HRS states at 0.2 V. The retention curve is given in figure. 7.2 (c). The curve shows that the retention window between LRS and HRS is maintained throughout the measurement. This analysis indicates that these devices are non-volatile and have potential to be used in NVM devices. Further, reliability of devices is ensured by plotting Weibull's distribution curve for V_{set} and V_{reset} voltages. The Weibull's distribution function is defined as

$$\ln[-\ln\{1-F(V)\}] = \beta\ln(V); \quad (7.1)$$

where β is shape parameter and higher value of β implies highly reliable device and F(V) is the function of set and reset voltage (Lawless, 1983). The estimated value of β for set and reset voltages are 6 and 11 respectively. The observed variation in reset voltage is in the range of -0.9 V to -1.5 V and that for set voltage in 0.9 V to 1.3 V. The statistical calculated average values of set and reset voltage is 1.15 V and -1.4 V, respectively.

The current conduction mechanism is investigated by plotting logarithmic curve of I-V for set and reset states to understand the switching mechanism. The logarithm I-V curve of set and reset sates are presented in figure 7.3 (a) & (b). The HRS of set state is divided into three regions by linear fitting which are , Ohmic region ($I \propto V$); Child's law region ($I \propto V^m$; $m = 2$); and sharp current increase region (X. Chen et al., 2009)(Chen et al., 2008). This conduction mechanism is attributed to space charge limited (SCLC) conduction mechanism. This mechanism tells that at lower voltage, thermally generated carrier dominants over the injected carrier and hence, the carriers follow Ohm's law. The injected carriers initially have large relaxation time and hence do not flow through the entire film thickness and follows Ohm's law. Further, when the voltage increases, injected charge carriers also increases and it fills the trap sites available in the film. This phenomenon brings the device to Child's law region. Filling of all the trap sites allow the injected carrier to move freely throughout the film, which brings the device in LRS mode. The Ohm's and Child's law region are defined by the formula $J_{Ohm} = qn_0\mu\frac{V}{d}$ and $J_{Child} = \frac{9}{8}\mu\varepsilon\frac{V^2}{d^3}$; where q is electronic charge, n_0 is free carrier concentration at thermal equilibrium, μ is electron mobility, V is bias voltage, d is film's thickness and ε is dielectric constant (Chiu, 2014).

The logarithmic curve of LRS in set region substantiates the Ohmic conduction mechanism, figure 7.3 (a). The ohmic conducting mechanism in LRS and SCLC conduction mechanising in HRS substantiates that the conduction is happening through a filament. Hence, switching mechanism is attributed to filament model. The results indicate that the charge is flowing through confined filament rather than homogenous distribution, indicating smaller size of filament in comparison to the area of the memory device(Yang et al., 2009). This result enables the probability to realize high density memory cells in this device configuration. Reset state showed similar conduction mechanism in both LRS and HRS states substantiating the conduction through filament, Fig. 7.3(b).

The filament model using SCLC conduction mechanism is reported for both oxygen vacancies migration and ion migration based filament(Sarkar et al., 2016)(Zhu et al., 2017). In our case, BFO might have oxygen vacancies as it depends on the growth conditions, however, we have used active Ag metal as TE which has tendency to migrate inside the film at low applied voltage. Also, it is reported that filament formation in RRAM devices with TE as active metal is usually due to metal ion migration under applied bias voltage, forming a conducting bridge between TE and BE(Yang et al., 2012)(Valov and Waser, 2013). Based on these reports,

we inferred that the switching in our Ag/BFO/FTO RRAM device is probably due to filament formation from migrating silver ions.

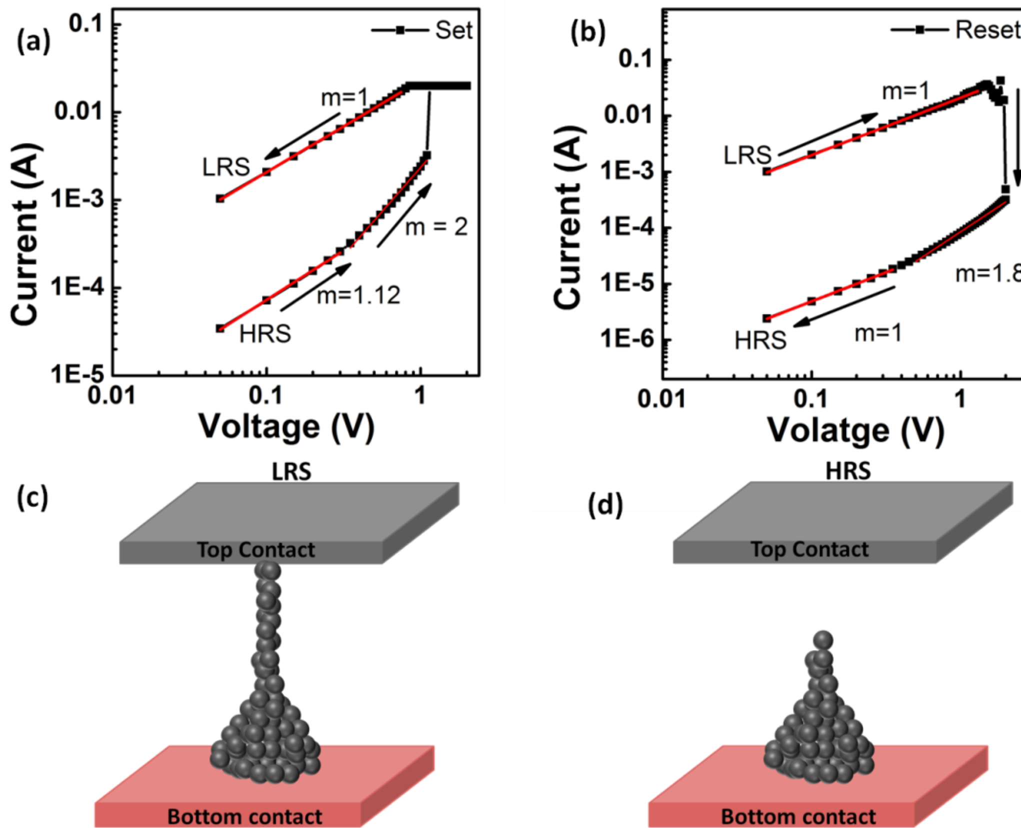

Figure 7.3: Logrithmic I-V curves for (a) Set and (b) Reset states; Schematic of (c) Filament formation and (d) Filament rupture

In CBRAM, initially the applied positive bias oxidizes Ag metal owing to its low work function. Oxidation results in silver ion as $Ag \rightarrow Ag^+ + e^-$. Further, increase in applied voltage pushes these Ag^+ ions towards BE by allowing it to pass through thin BFO film. At the bottom electrode, the Ag^+ ions recombine with electrons supplied by FTO and become $Ag^+ + e^- \rightarrow Ag$, forming Ag atoms. These Ag atoms deposited on BE accumulates and further grow towards TE, constructing a conducting filament from BE to TE at V_{set}, as schematically shown in Fig 7.3 (c) (Guo et al., 2007). This conducting filament turns the devices from HRS to LRS and causes the onset of ON state of RRAM device. When the bias polarity is reversed, Ag filament starts dissolving near the TE, owing to Joules' heating effect due to the maximum power dissipation at the thinnest part of the filament. This process brings the devices from HRS to LRS and turns the device OFF, as schematically explained in Fig 7.3 (d).

Further, robustness of the devices is ensured by checking its working after 10 months of fresh device fabrication. Throughout the months, these devices were kept at ambient environmental conditions. The devices sustained its bipolar switching characteristics and exhibits invariant reproducibility for 100 cyclic operations, Fig 7.4 (a). The devices maintained its resistance in LRS and HRS for 10^3 seconds without any degradation ensuring its retained non-volatility, Fig 7.4 (b). Further, stability of these devices is ensured by endurance measurement with a square electric pulse of set and reset voltage at +1.3 V and -1.3 V, respectively. The estimated pulse width of the electric pulse is 100 ms. The endurance measurement is investigated for 1000 cycles and the results substantiate devices' consistency in HRS and LRS sates, ensuring its stability, Fig 7.4 (c). The endurance resistance window in ON and OFF state is well maintained for the entire cycle range. The working of devices after

endurance is ensured by measuring another cyclic I-V, Fig 7.4 (d). The device gain showed similar bipolar RRAM characteristic as the fresh sample which substantiates that these devices have potential to realize highly stable and reliable RRAM memory cells.

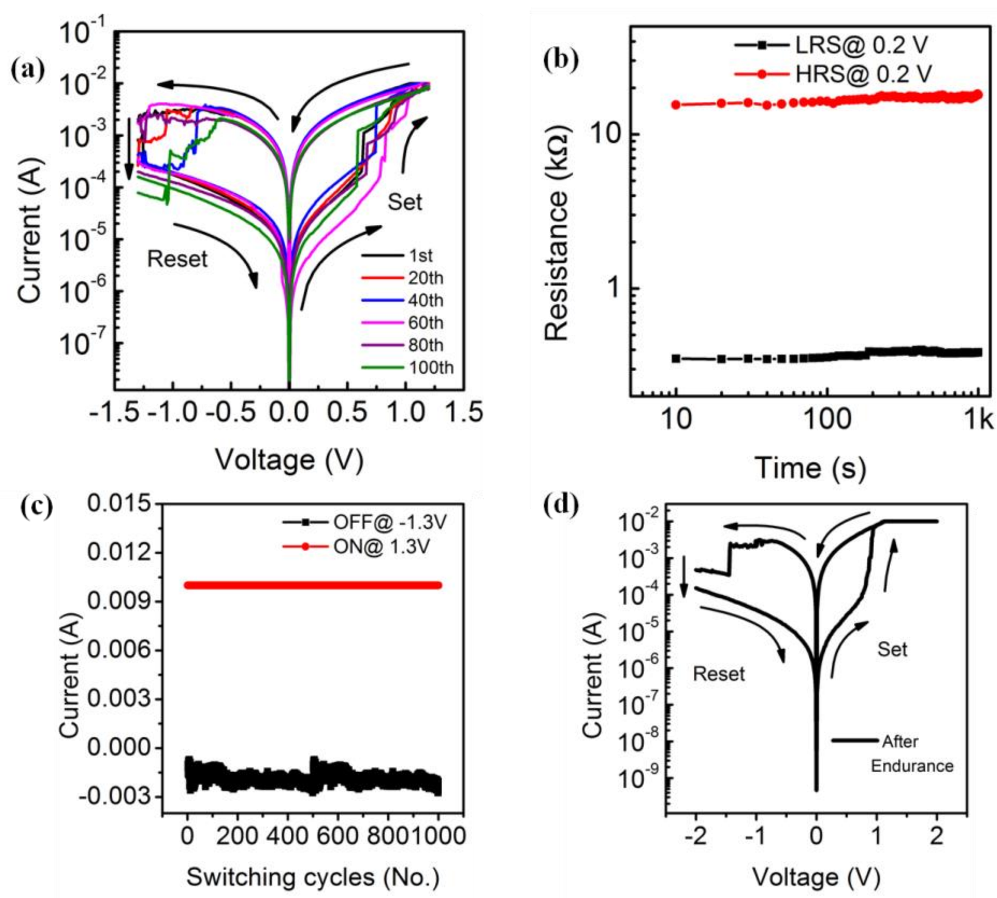

Figure 7.4 : (a) I-V plot of RRAM device after 10 months for multiple cycles, (b) Retention graph, (c) Endurance curve for 1000 cycles and (d) Switching cycle after endurance.

7.4 Conclusion

In summary, we have synthesized a low cost and simple sol-gel derived phase pure BFO film on FTO coated glass. The RRAM properties of Ag/$BiFeO_3$/FTO device configuration indicate a bipolar, non-volatile memory device with large I_{on}/I_{off} ratio ~ 450. The device maintained its retention window for 10^4 s and smaller switching set and reset voltage is observed ~ 1.1 V and -1.5 V, respectively. The devices exhibit excellent reproducibility for 100 cycles. The current conduction mechanisms is attributed to ohmic and SCLC for LRS and HRS regions, respectively. The switching mechanism is assigned to formation and rupture of silver filament. The reliability curve indicates smaller variation in set and reset voltage. The robustness test of the devices suggests that these devices are reproducible and non-volatility is maintained. The endurance test of these devices indicates that these devices are stable. The robustness measurements after 10 months of first fabrication substantiate environmental stability of these devices.